Best Student Paper Award

Hybrid silicon-plasmonics: Efficient waveguide interfacing for low-loss integrated switching components

Odysseas Tsilipakos, Alexandros Pitilakis, Emmanouil E. Kriezis

Department of Electrical and Computer Engineering, Aristotle University of Thessaloniki, Thessaloniki GR-54124, Greece.

ABSTRACT

We present a thorough numerical investigation of end-fire coupling between dielectric-loaded surface plasmon polariton (DLSPP) and compact rib/wire silicon-on-insulator (SOI) waveguides. Simulations are based on the three-dimensional vector finite element method. The interface geometrical parameters leading to optimum performance, i.e., maximum coupling efficiency or, equivalently, minimum insertion loss (IL), are identified. We show that coupling efficiencies as high as 85 % are possible. In addition, we quantify the fabrication tolerances about the optimum parameter values. In the same context, we assess the effect of a metallic stripe gap and that of a horizontal offset between waveguides on insertion loss. Finally, we demonstrate that by benefiting form the low-loss coupling between the two waveguides, hybrid silicon-plasmonic 2×2 thermo-optic switching elements can outperform their all-plasmonic counterparts in terms of IL. Specifically, we examine two hybrid SOI-DLSPP switching elements, namely, a Mach-Zehnder Interferometer (MZI) and a Multi-Mode-Interference (MMI) switch. In particular, in the MZI case the IL improvement compared to the all-plasmonic counterpart is 4.5 dB. Moreover, the proposed hybrid components maintain the high extinction ratio, small footprint, and efficient tuning traits of plasmonic technology.

Keywords: Optical waveguide junction, dielectric-loaded plasmonic waveguide, silicon on insulator waveguides, hybrid silicon-plasmonics, Mach-Zehnder interferometer, multi-mode interference switch, thermo-optic effect.

1. INTRODUCTION

Guided-wave plasmonics have attracted considerable interest in recent years.[1] Both passive and active components have been examined, in pursuit of nanoscale dimensions and/or high energy efficiency; the latter usually stemming from field enhancement at metal-dielectric interfaces. However, for such desirable features there is a price to be paid, namely, high propagation losses associated with field penetration in metal regions. Thus, significant effort has been directed in reducing or compensating for the inherent resistive losses of plasmonic waveguides, through elaborate geometrical/material configurations[2] or by introducing materials with gain,[3,4] respectively. Nevertheless, the high insertion loss (IL) of plasmonic components still remains the bottleneck of their performance. Therefore, a simple idea emerged:[5] using plasmonic components only where small footprint and/or high efficiency is required and leaving the interconnection of such components to low-loss photonic waveguides. In other words, hybrid plasmonic-photonic circuits, instead of all-plasmonic ones, are currently considered the most promising approach for efficient nanophotonic circuitry. Obviously, for such circuits to become a reality, efficient interfacing of plasmonic and photonic waveguides is a necessary prerequisite.

To date, several plasmonic-photonic waveguide transitions have been examined based on either end-fire or directional coupling schemes. In the first case, spatial matching of the mode profiles is what mainly determines coupling efficiency, whereas in the second, it is phase matching that becomes the primary concern, since phase-constant disparity limits the maximum possible power exchange. Initially, studies revolved around the stripe plasmonic waveguide, since it was the first 2D plasmonic waveguide, i.e., able to confine light in both transverse directions, to be extensively investigated. Coupling to standard silica fibers[6] and planar dielectric waveguides[7] were progressively considered. However, the long-range mode supported by the stripe plasmonic waveguide lacks strong lateral confinement and therefore cannot serve the purpose of densely integrated circuits. Thus, efforts have

E-mail addresses: otsilipa@auth.gr; alexpiti@auth.gr; mkriezis@auth.gr

Nanophotonics IV, edited by David L. Andrews, Jean-Michel Nunzi, Andreas Ostendorf,
Proc. of SPIE Vol. 8424, 84241E · © 2012 SPIE · CCC code: 0277-786X/12/$18
doi: 10.1117/12.922298

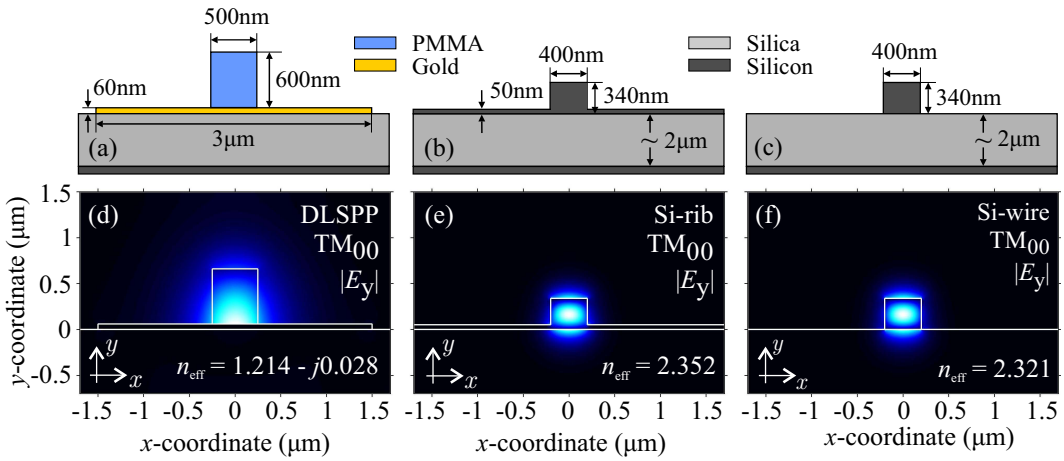

Figure 1. (a)-(c) DLSPP, Si-rib, and Si-wire waveguide cross-sections. All dimensions are in scale except for the BOX thickness. (d)-(f) Distribution of the dominant E-field component (absolute value) for the fundamental quasi-TM mode of DLSPP, Si-rib, and Si-wire waveguides. The corresponding effective indices are also included.

recently concentrated on plasmonic waveguides exhibiting stronger confinement.[8–11] Specifically, these include wire,[8] slot,[9] hybrid silicon-plasmonic,[10] and dielectric-loaded surface plasmon polariton (DLSPP)[11] waveguides.

Among the aforementioned plasmonic waveguides, the DLSPP is the most extensively investigated. It has been employed in the implementation of a broad range of passive components. More importantly, DLSPP-based switching elements relying on the thermo-optic effect have been recently demonstrated.[12–14] In addition, the DLSPP waveguide is technologically simple and exhibits relatively small propagation losses. Specifically, the propagation length, i.e., the e-folding distance of the optical intensity, is in the order of 50 μm for the fundamental TM_{00} mode. At first, an attempt to access DLSPP waveguides via standard single-mode fibers was made.[15] This allowed for accurate fiber-to-fiber characterization of DLSPP-based components.[16] Obviously, coupling to fibers does not serve the purpose of planar hybrid plasmonic-photonic circuits. Therefore, an end-fire approach for coupling light between DLSPP and planar silicon-on-insulator (SOI) waveguides has been recently demonstrated.[11] However, a thorough numerical investigation of the waveguide interface has yet to be performed. Moreover, the rib silicon waveguide of Ref. 11 is rather bulky and thus a different choice for the SOI waveguide could prove advantageous, provided, of course, that the coupling efficiency is equally good.

In this work, we thoroughly analyze the performance of end-fire coupling between the DLSPP and a compact SOI waveguide. Both rib and wire variants of the SOI waveguide are examined, and a comparison between the two is provided. In each case, the geometrical parameters of the interface are varied in order to identify the ones leading to optimum performance, i.e., maximum coupling efficiency or, equivalently, minimum insertion loss. In addition, we assess the effect of a longitudinal metallic stripe gap and that of a horizontal offset between waveguides on insertion loss, since such scenarios can arise in fabricated structures as a result of resolution limitations and misalignment errors. Finally, we examine two hybrid SOI-DLSPP switching elements, namely, a Mach-Zehnder Interferometer (MZI) and a Multi-Mode-Interference (MMI) switch. Benefiting from the low-loss coupling between the two waveguides, such components feature reduced IL compared to their all-DLSPP counterparts.

2. DLSPP AND RIB/WIRE SOI WAVEGUIDES

Fig. 1(a)-(c) depicts the cross-sections of DLSPP and rib/wire SOI waveguides. Specifically, the DLSPP waveguide [Fig. 1(a)] consists of a 500 nm $\times$ 600 nm poly-methyl-methacrylate (PMMA) ridge on top of a 3 μm $\times$ 60 nm gold stripe. The combined structure of ridge and stripe resides on a typical silicon-on-insulator (SOI) substrate with a buried oxide (BOX) thickness of 2 μm (dimension not in scale). For such ridge dimensions, the DLSPP waveguide is single-mode at telecom wavelengths. On the other hand, the SOI waveguide consists of a 400 nm $\times$ 340 nm silicon core on top of the same SOI substrate. The height value of 340 nm ensures that the

fundamental quasi-TM mode is tightly confined inside the silicon core. In the rib case [Fig. 1(b)], the silicon layer is deeply etched outside the core region, leaving a 50-nm-thick silicon slab. In the wire case [Fig. 1(c)] the silicon layer is etched all the way down to the oxide. For the said core dimensions, the SOI waveguide is not single-mode; the fundamental quasi-TE mode is also supported. However, the symmetry of the DLSPP mode field components dictates that coupling only to the fundamental quasi-TM mode of the SOI waveguide is actually possible. Finally, as far as the material parameters are concerned, the refractive indices of all materials involved at the working wavelength of 1.55 μm are: $n_{\mathrm{PMMA}} = 1.493$, $n_{\mathrm{Gold}} = 0.55 - j11.5$,[17] $n_{\mathrm{Silica}} = 1.45$, and $n_{\mathrm{Silicon}} = 3.45$.

In Fig. 1(d)-(f) we plot the dominant electric field component (E_y) for the fundamental quasi-TM modes of the waveguides. Notice that the mode distributions and effective indices of rib and wire variants are very similar. However, this is true only for rather large core widths, as is the nominal value of 400 nm. As will become evident in Sec. 3.2, the presence or absence of a silicon slab has a stronger impact on mode distribution for smaller widths. Clearly, spatial matching of the DLSPP and SOI waveguide mode profiles is not particularly good. Specifically, the x-extent of the DLSPP mode is almost double that of the SOI mode. Furthermore, the two modes are not centered along the y-axis. As a result, the lower part of the SOI mode cannot contribute to coupling, since it is shadowed by the metallic stripe. Thus, it seems that both broadening the SOI mode along the horizontal (x) direction, as well as centering the two modes with respect to the vertical (y) direction are required in order to improve spatial matching. Broadening of the SOI mode can be actually accomplished by reducing the rib width, as this tends to relax mode confinement, whereas centering along the y direction can be provided by some kind of vertical offset between the two waveguides. Therefore, in what follows, certain dimensions of the interface are allowed to vary, in pursuit of optimum performance, i.e., maximum coupling efficiency or, equivalently, minimum insertion loss.

3. DLSPP TO SOI WAVEGUIDE TRANSITION

In order to determine the coupling efficiency between the two waveguides (more specifically between their fundamental TM-like modes), we consider a DLSPP to SOI waveguide transition [Fig. 2(a)], meaning that light is impinging on the waveguide interface from the DLSPP waveguide. The opposite direction of propagation has been also examined, yielding very similar results. This is consistent with Ref. 18, which states that the coupling efficiency between two specific guided modes is reciprocal, even if other modes, guided or radiation ones, are excited at the interface. Note, however, that in such cases other quantities such as the return loss or total guided power, seize to be reciprocal.[18] All simulations are performed by means of an in-house implementation of the three-dimensional vector finite element method (3D-VFEM).[19,20]

We now briefly comment on the procedure followed for calculating the coupling efficiency (insertion loss). Clearly, the DLSPP mode, besides exciting the fundamental guided mode of the Si-rib waveguide (TM_{00}), excites radiation modes as well. This is true especially for those geometrical parameter combinations leading to non-optimum spatial matching of the two TM_{00} modes. Therefore, while calculating the output power one should take extra care in distinguishing between the useful power carried by the TM_{00} Si-rib mode and power coupled to radiation modes which, obviously, should not enter in the result. For this purpose, a vector overlap integral exploiting mode orthogonality:

$$OI(z) = \frac{\left| \iint_A \mathbf{E}(x,y,z) \times \mathbf{H}^*_{\mathrm{ref}}(x,y) \cdot \hat{\mathbf{z}}\, dx\, dy \right|^2}{\left| \iint_A \mathbf{E}(x,y,z) \times \mathbf{H}^*(x,y,z) \cdot \hat{\mathbf{z}}\, dx\, dy \right| \left| \iint_A \mathbf{E}_{\mathrm{ref}}(x,y) \times \mathbf{H}^*_{\mathrm{ref}}(x,y) \cdot \hat{\mathbf{z}}\, dx\, dy \right|} \tag{1}$$

is evaluated along the output (Si-rib) waveguide. Specifically, at each z-coordinate the actual propagating field $\mathbf{E}(x,y,z)$ is correlated with a reference field $\mathbf{H}_{\mathrm{ref}}(x,y)$, namely, the TM_{00} Si-rib mode specified from the solution of a 2D eigenvalue problem of the waveguide cross-section, and properly normalized. The result of Eq. (1) is the fraction of the total guided power carried by the TM_{00} mode. Thus, by using this overlap integral to scale the total guided power, found by integrating the time-averaged Poynting vector over the waveguide cross-section, we can correctly determine the output power and, consequently, the insertion loss. Finally, we note

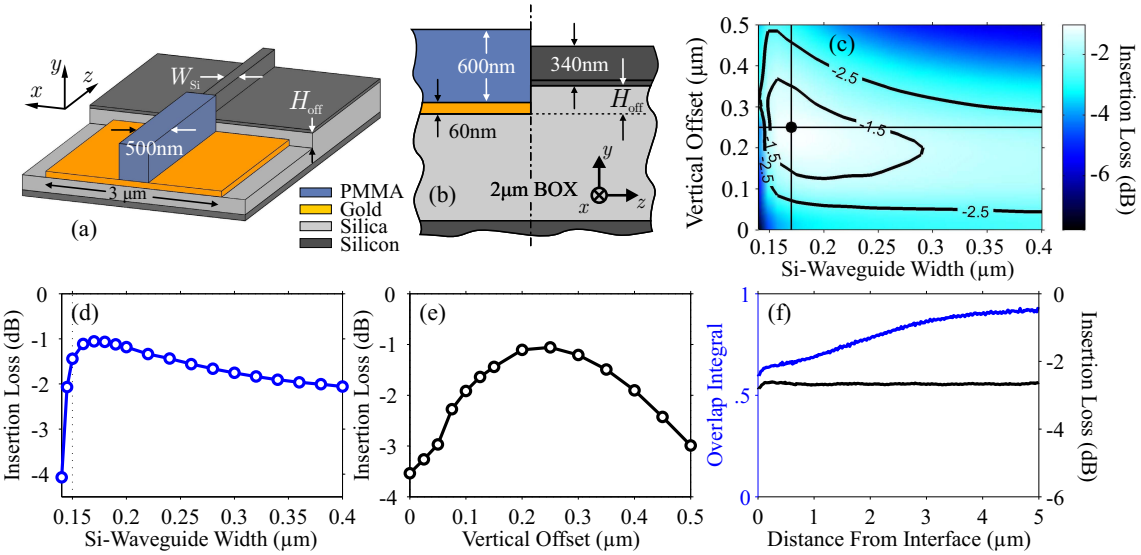

Figure 2. Schematic of DLSPP to Si-rib waveguide transition: (a) bird's eye view and (b) side view. Performance of DLSPP to Si-rib waveguide transition: (c) Insertion loss (IL) as a function of Si-rib width (W_{Si}) and vertical offset (H_{off}). The optimum point in W_{Si}-H_{off} space is clearly marked and corresponds to (W_{Si}, H_{off}) = (170 nm, 250 nm). (d) IL vs W_{Si} for optimum value of H_{off}. (e) IL vs H_{off} for optimum value of W_{Si}. (f) Overlap integral and IL calculated along the output waveguide. W_{Si} is set at its nominal value (400 nm) and no vertical offset is provided. Although the overlap integral requires more than 5 μm of output waveguide length to approach unity, IL calculation can be safely performed even after less than 1 μm in the output waveguide.

that in calculating the insertion loss of the waveguide junction, the propagation losses of the DLSPP mode are compensated for. This is done by artificially restoring the losses suffered during propagation in the DLSPP section of the waveguide transition under examination.

3.1 Si-rib Waveguide

We first focus on a DLSPP to Si-rib waveguide transition. Schematics of the simulated structure along with the relevant geometrical parameters are depicted in Fig. 2(a),(b). In order to design an efficient transition, we have allowed for a vertical offset between the two waveguides. This offset, H_{off}, is simply the etch depth of the buried oxide layer in the DLSPP side of the transition [Fig. 2(b)]. To the same end, we have allowed for another degree of freedom, namely, the width of the silicon rib at the interface, W_{Si} [Fig. 2(a)]. We assume that the silicon waveguide is adiabatically tapered from the nominal width of 400 nm over a sufficiently long distance prior to reaching the interface, so as to ensure minimal tapering losses. The dimensions of PMMA ridge and gold stripe as well as the silicon rib thickness are fixed to their nominal values, already presented in Sec. 2.

First, a parametric analysis with respect to both W_{Si} and H_{off} is performed, in order to identify the parameter values leading to optimum performance. The results are depicted in Fig. 3(c). Minimum insertion loss is attained for (W_{Si}, H_{off}) = (170 nm, 250 nm) and equals -1.05 dB. Such an IL value corresponds to a coupling efficiency of 80 %, equally good to the one reported in Ref. 11. As anticipated, optimum performance demands both reducing the Si-rib width, in order to broaden the supported mode, as well as providing a significant vertical offset, in order to center the modes vertically.

Next, we plot the IL as a function of each design parameter while keeping the other constant at its respective optimum [Fig. 3(d),(e)]. This way we can determine the fabrication tolerance about the optimum values. Specifically, Fig. 3(d) depicts the dependence on W_{Si} when H_{off} is at its optimum (250 nm). For widths ranging between $150 - 250$ nm the dependence is rather weak (IL remains better than -1.5 dB), indicating ample fabrication tolerance. The no-tapering penalty, i.e., the extra IL suffered should the waveguide width be left at its nominal value (400 nm), is 1 dB. We should also note that the steep IL increase for widths below 145 nm is due to the fact that for such widths the supported mode severely lacks confinement and eventually becomes leaky.

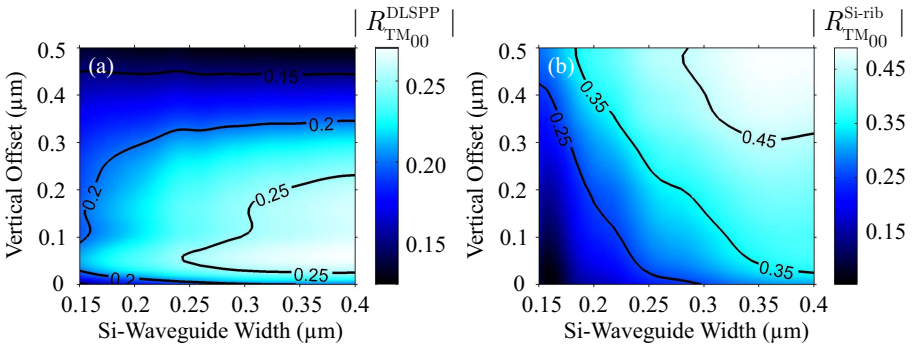

Figure 3. Amplitude reflection coefficients (absolute value) calculated for the fundamental TM_{00} mode of the input waveguide for both propagation directions: (a) DLSPP to Si-rib waveguide transition and (b) Si-rib to DLSPP waveguide transition.

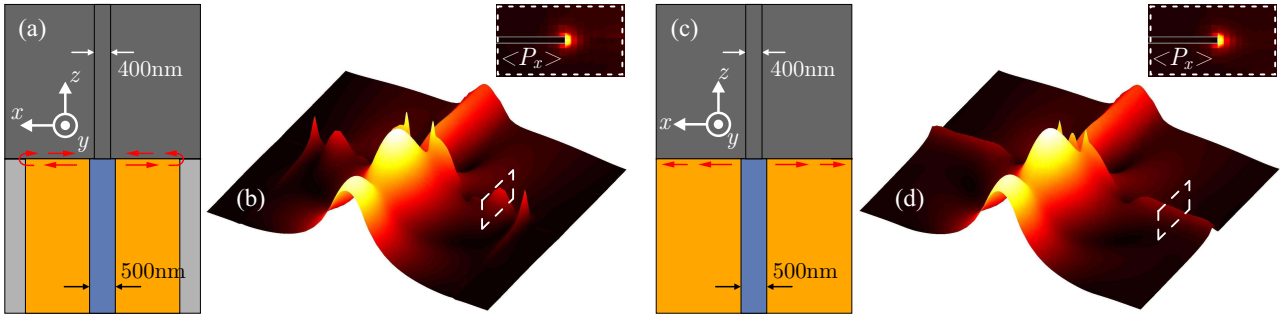

Figure 4. Edge SPPs guided along the stripe border for a DLSPP to Si-rib waveguide transition with nominal rib width and no vertical offset. Finite stripe width: (a) Top view schematic. The arrows indicate the route of edge SPPs. (b) Distribution of E_y component (absolute value) on xz-plane just above the metallic film. Edge SPPs are guided parallel to the interface until reaching the stripe corner where they are reflected forming a standing wave pattern. Infinite stripe width: (c) Top view schematic. The arrows indicate the route of edge SPPs. (d) Distribution of E_y component (absolute value) on xz-plane just above the metallic film. Edge SPPs are guided parallel to the interface until exiting the computational domain.

In the same way, Fig. 3(e) depicts the dependence on H_{off} when W_{Si} is fixed at its respective optimum (170 nm). Again, fabrication tolerance is ample. Specifically, IL remains better than -1.5 dB for vertical offsets ranging between $150 - 350$ nm. The no-offset penalty, i.e., the extra IL suffered in case no vertical offset is provided, is 2.5 dB. Let us also note that the abrupt jump in IL when the vertical offset exceeds the value of 60 nm (equal to metal stripe thickness) is associated with the lower part of the Si-rib mode contributing to coupling.

As discussed earlier, by following a procedure involving the computation of a vector overlap integral given by Eq. (1), we can safely calculate the insertion loss at almost any point along the output waveguide, even if radiation modes are still present. This is demonstrated in Fig. 2(f) depicting the overlap integral and insertion loss along the output waveguide. The Si-rib waveguide is left at its nominal width (400 nm) and no vertical offset is provided. Spatial matching of the two TM_{00} modes is not particularly good, leading to the excitation of radiation modes and yielding an insertion loss of approximately 2.7 dB. More than 5 μm in the output waveguide are required for the radiation modes to leave the computational domain and the overlap integral to approach unity. However, even less than a micrometer after the waveguide interface the insertion loss can be safely calculated.

Regarding reflection from the interface, the 3D-FEM solution permits a rigorous calculation of the reflection coefficient associated with the fundamental mode of the input waveguide ($R_{TM_{00}}$). In Fig. 3 we plot the absolute value of such amplitude reflection coefficients as a function of W_{Si} and H_{off} for both DLSPP-to-SOI and SOI-to-DLSPP propagation directions. When impinging on the interface from the DLSPP waveguide, values ranging

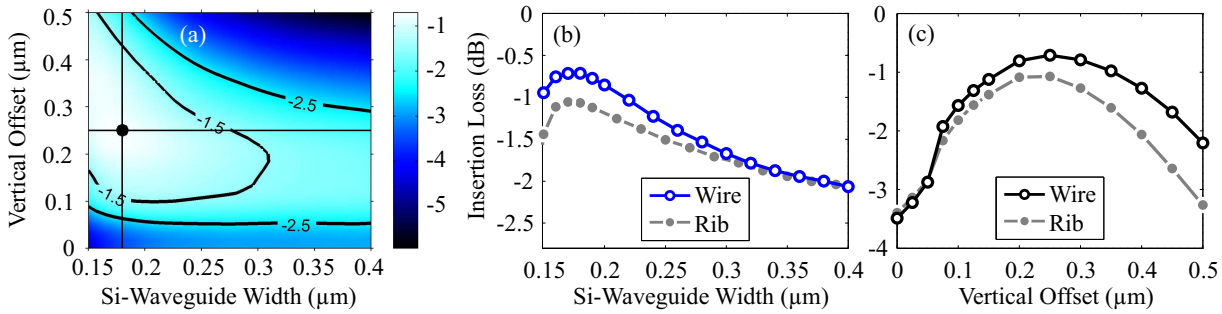

Figure 5. Performance of DLSPP to Si-wire waveguide transition without a longitudinal metallic stripe gap: (a) Insertion loss (IL) as a function of Si-rib width (W_{Si}) and vertical offset (H_{off}). The optimum point in W_{Si}-H_{off} space is clearly marked and corresponds to (W_{Si}, H_{off}) = (180 nm, 250 nm). (b) IL vs W_{Si} for optimum value of H_{off}. (c) IL vs H_{off} for optimum value of W_{Si}. In both cases, IL curves corresponding to Si-rib waveguides of identical dimensions are also included for comparison purposes.

from 0.125 to 0.27 are obtained [Fig. 3(a)]. This means that depending on the geometrical parameter settings, approximately $1.5-7.3$ % of the input power is reflected from the interface in the form of the fundamental mode. All of the remaining power would couple to the fundamental mode of the output waveguide if it were not for (transmitted/reflected) radiation modes and (to a much lesser extent) edge SPPs guided along the metallic stripe border (Fig. 4). SPPs guided parallel to the interface of a waveguide junction have been also observed in Ref. 8. As an example, in the optimum case where coupling efficiency is 80 %, approximately 4 % of the impinging power is reflected from the interface in the form of the fundamental mode, whereas the remaining 16 % is mainly lost to transmitted radiation modes. On the other hand, when impinging on the interface from the Si-rib waveguide the reflection coefficients are in general higher [Fig. 3(b)]. This means that a larger portion of the input power, up to 24 %, is reflected from the interface, while less is coupled to radiation modes. Clearly, the comparison of the reflection coefficients for the two propagation directions reveals that when radiation modes are excited on a waveguide junction, return loss is not reciprocal.

3.2 Si-wire Waveguide

Let us now focus on the wire variant of the SOI waveguide. For the analysis of the DLSPP to Si-wire waveguide transition, we follow a procedure identical to that of Section 3.1. First, a parametric analysis with respect to W_{Si} and H_{off} is conducted and the optimum point in W_{Si}-H_{off} space is identified [Fig. 5(a)]. It corresponds to (W_{Si}, H_{off}) = (180 nm, 250 nm) and the respective IL equals -0.7 dB (coupling efficiency of 85 %). This constitutes a 0.35-dB improvement with respect to the rib case. The contour lines in Fig. 5(a) indicate that fabrication tolerances about the optimum parameter settings are ample.

Next, the IL dependence on each design parameter is separately examined. In Fig. 5(a) we plot the IL as a function of W_{Si}, while keeping H_{off} fixed at its optimum (250 nm). In the same way, Fig. 5(b) depicts the dependence on H_{off} when W_{Si} is fixed at its own optimum (180 nm). Insertion loss curves corresponding to the rib variant of the transition (identical geometrical parameters) are included for comparison purposes. As can be seen, IL remains better than -1.5 dB for widths up to 280 nm and offsets ranging from 100 to 430 nm.

By observing Fig. 5(b) one can verify that for the nominal core width the two SOI waveguide variants yield almost identical insertion losses. This comes as no surprise since for large core widths the mode profiles of wire and rib variants are very similar, as already mentioned [Fig. 1(b),(c)]. However, for smaller widths the presence/abscence of a silicon slab has a stronger impact on field distribution, and consequently on the spatial matching with the DLSPP mode. This explains the different coupling efficiencies in narrow SOI waveguide cases [Fig. 5(b),(c)]. Finally, regarding reflection from the interface we note that the results are very similar (trends and extreme values) to those obtained for the rib variant of the SOI waveguide (Fig. 3).

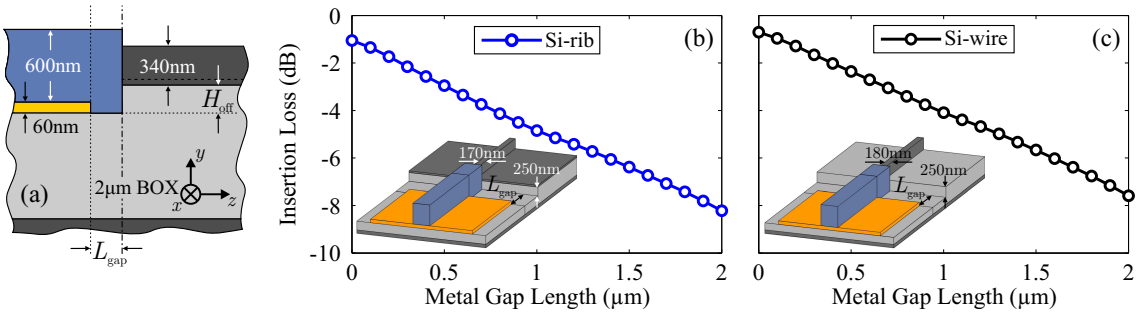

Figure 6. (a) Side view of DLSPP to SOI waveguide transition with a metal stripe gap. Notice that the metallic stripe does not reach the waveguide interface but stops a distance L_{gap} before it. Insertion loss versus metallic stripe gap length: (b) DLSPP to Si-rib and (c) DLSPP to Si-wire waveguide transitions.

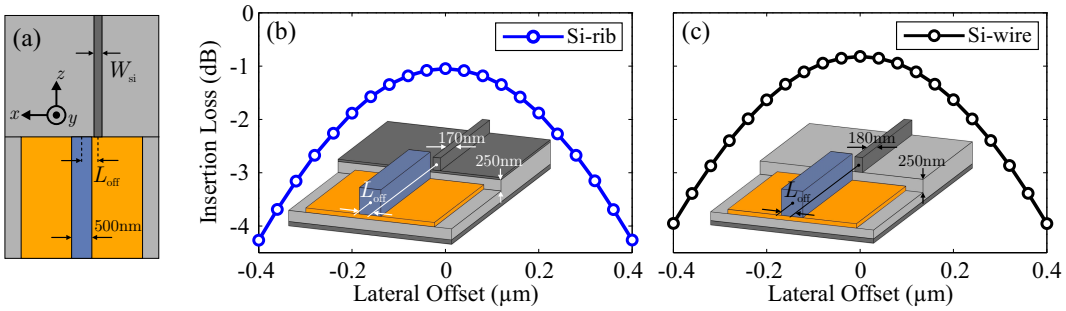

Figure 7. (a) Top view of DLSPP to SOI waveguide transition with a horizontal (lateral) offset between waveguides (L_{off}). Insertion loss versus L_{off}: (b) DLSPP to Si-rib and (c) DLSPP to Si-wire waveguide transitions. In both cases, a lateral offset of 0.2 μm corresponds to an IL penalty of approximately 1 dB.

4. PRACTICAL CONSIDERATIONS

In this section, we investigate two scenarios which could arise in fabricated samples as a result of misalignment errors and/or resolution limitations. Specifically, we examine the effect on insertion loss of a longitudinal metallic stripe gap and that of a horizontal offset between the guides.

4.1 Longitudinal Metallic Stripe Gap

First, we focus on the effect of a longitudinal metallic stripe gap on insertion loss. A side view of the simulated structure is depicted in [Fig. 6(a)]. Note that the metallic stripe does not reach the waveguide interface but stops a distance L_{gap} before it. In order to assess the effect of the gap on IL, we fix W_{Si} and H_{off} at their optimum values and let L_{gap} vary from 0 to 2 μm. The results are depicted in Fig. 6(b),(c) for rib and wire SOI waveguides, respectively. In the first case, a 0.5-μm gap leads to ILs of -2.95 dB [Fig. 6(b)], whereas in the second, the same gap value leads to an IL of -2.35 dB. Note that the wire outperforms the rib more significantly compared to the no-gap case. Specifically, the IL improvement is 0.6 dB instead of 0.35 dB (Sec. 3.2). As the gap length increases beyond 0.5-μm, the IL becomes quite high. For example, in the extreme case of a 2-μm gap the IL reaches a value of approximately 8 dB for both SOI waveguide variants. This, however, comes as no surprise since the waveguide formed by the 500 nm $\times$ 660 nm polymer ridge on top of a silica substrate cannot sustain a guided mode. As a result, field components are bound to spread over the extent of the gap, meaning that coupling to the SOI waveguide at the waveguide interface will suffer heavy losses.

4.2 Horizontal Offset

Next, we investigate the effect of a horizontal (lateral) offset, L_{off}, between guides. Fig. 7(a) depicts a top view schematic of the structure. We fix W_{Si} and H_{off} at their optimum values and vary L_{off}. In Fig. 7(b),(c) we plot the corresponding results for rib and wire waveguides, respectively. As can be seen, in both cases offsets in the

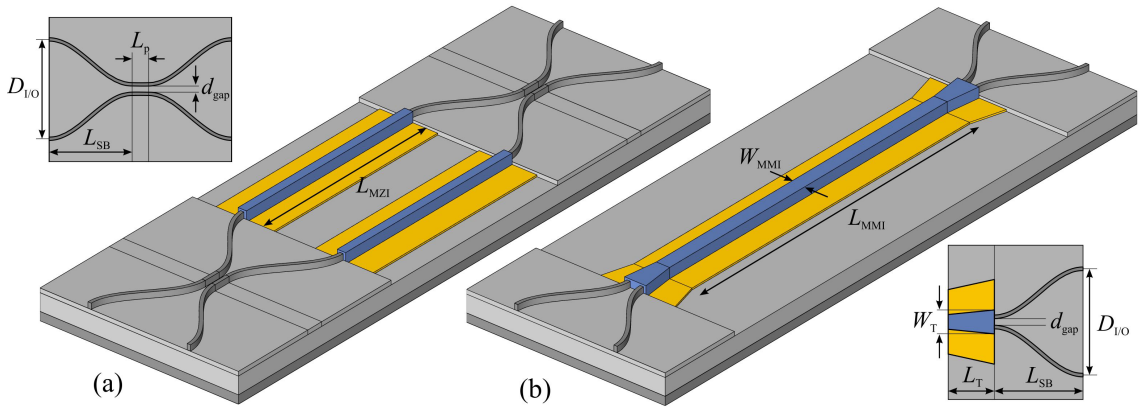

Figure 8. Bird's eye view of hybrid SOI-DLSPP 2×2 switching elements: (a) MZI and (b) MMI configurations. Top view schematics of the MZI 3 dB-coupler and MMI Y-junction along with the relevant geometrical parameters are included as insets.

order of 50 nm do not significantly affect the IL. On the other hand, a horizontal offset of 0.2 μm corresponds to an IL penalty of 1 dB, whereas, an 0.4-μm offset leads to an IL penalty of approximately 3 dB.

5. HYBRID SOI-DLSPP SWITCHING ELEMENTS

Having assessed the efficiency of end-fire coupling between DLSPP and SOI waveguides, we investigate its potential for hybrid silicon-plasmonic components. Please note that in the present context, the term "hybrid silicon-plasmonics" is used to describe integrated components made up of two distinct waveguide types, namely, plasmonic (DLSPP) and photonic (SOI). This should not be confused with recently-proposed hybrid silicon-plasmonic waveguides,[10] who themselves comprise metal as well as silicon regions in order to benefit from both plasmonic and high-index-contrast confinement mechanisms. Specifically, we explore how this efficient waveguide interface can be used to improve the performance of existing all-DLSPP 2×2 switching elements based on the thermo-optic effect.[13]

The switching configurations we will consider are the Mach-Zehnder Interferometer (MZI) and the Multi-Mode Interference (MMI) switch. The performance bottleneck of the all-DLSPP designs is the increased IL.[13] This comes as no surprise as the typical component length is larger than the propagation length of the DLSPP waveguide. However, one can point out that the lossy plasmonic waveguides are necessary only in the sections of the component where the thermo-optic effect is used for the switching; all other sections are passive routing elements, namely, 3 dB-couplers, Y-junctions and I/O-feeds. We can thus implement these passive sections with low-loss silicon-photonic waveguides, instead of the DLSPP, and reduce the overall IL of the component. This is possible since the aggregate interfacing losses, suffered when passing from DLSPP to SOI waveguides and vice-versa, are smaller compared to the typical propagation losses along these passive plasmonic sections, were they implemented with the DLSPP waveguide.

5.1 Mach-Zehnder Interferometer

The proposed hybrid SOI-DLSPP MZI switch is depicted in Fig. 8(a). As can be seen, the input/output 3 dB-couplers are implemented with Si-wire instead of DLSPP waveguides. Obviously, the Si-rib variant can be used as well. In any case, the SOI waveguide width at the interface should allow for efficient coupling with the DLSPP waveguide. According to the findings of Sec. 3, the respective values for wire and rib waveguides are 180 nm and 170 nm. Therefore, we can either implement the entire 3 dB-coupler using these width values [Fig. 8(a)] or stick with the nominal 400 nm width and consequently taper the SOI waveguides prior to the waveguide interfaces. Designs for both cases will be provided in the following. Moreover, notice that the MZI arms are accommodated in a buried-oxide cavity providing the necessary vertical offset (250 nm) for efficient coupling between the two waveguides [Fig. 8(a)].

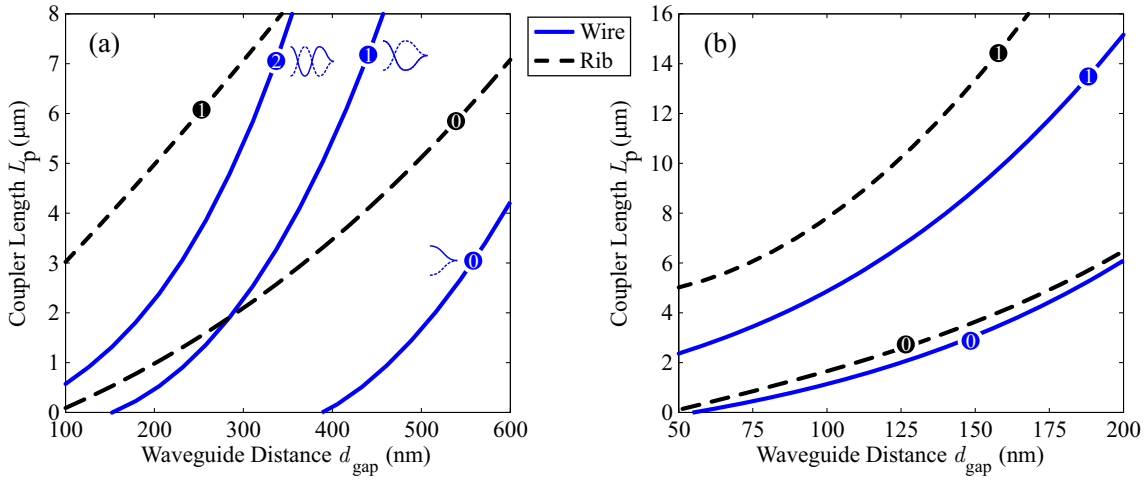

Figure 9. Design of silicon wire/rib 3 dB-couplers, for (a) the optimal width of 170 nm/180 nm and (b) the nominal width of 400 nm. For each gap between the waveguides in the parallel coupling region, we have calculated the necessary length to achieve 3 dB-splitting. The accessible coupling-orders are marked, identified by the number of times the power is exchanged before it is equally split between the two arms.

Before we get into specific design details, let us compare the proposed hybrid SOI-DLSPP MZI switch with the reference all-DLSPP one in terms of IL. If we employ Si-wire waveguides for the 3 dB-couplers, the aggregate interfacing losses are approximately 1.5 dB (Sec. 3.2). On the other hand, considering the reference longitudinal and lateral S-bend displacements of $L_{SB} = 10$ μm and $D_{I/O} = 6$ μm, respectively, the pair of DLSPP-based couplers is accompanied with aggregate propagation/radiation losses of approximately 6 dB.[13] Therefore, the IL improvement is 4.5 dB. An extra advantage of the hybrid component is that when implemented with SOI waveguides, the S-bends can be smaller. This is possible since the respective mode confinement is stronger and the waveguide can be bent over shorter distances with negligible radiation losses. Clearly, this leads to a reduced component footprint. Finally, we note that the remaining switching performance characteristics, such as ER, power consumption, and switching speed, are not affected by the different implementation of the 3 dB-couplers.

Regarding the thermo-optic design of the DLSPP parts of this component, the length of the MZI arms is given by $L_{MZI} = 0.5\lambda/\Delta n_{eff}$, where Δn_{eff} is the shift in the effective refractive index of the thermally-addressed arm, from its unheated value. This shift results from the polymer-index difference between the unheated and heated states, corresponding to the CROSS and BAR states of the symmetric 2×2 switch, respectively.[19] Next, we turn to the silicon-photonic 3 dB-couplers. For their design we employed a custom-built Finite-Element-Method (FEM) based Beam-Propagation-Method (BPM).[19] Our 3D-FE-BPM simulates the entire 3 dB-coupler taking fully into account the coupling between the two S-bent arms as they approach the parallel coupling section. This additional coupling is considerable in the case of small lateral gaps between the waveguides in the coupling section. Figure 9 presents the length of the parallel waveguide sections of the 3 dB-couplers (L_p) that is needed to achieve the desired 3 dB-splitting, as a function of the lateral gap distance of the arms (d_{gap}). We present a total of four designs, for both Si-wire and Si-rib waveguides, and for both the optimal and nominal silicon ridge widths (180/170 nm and 400 nm, respectively). In our designs the input/output feed-ports have a lateral separation of $D_{I/O} = 6$ μm and the sinusoidal S-bends have a length of $L_{SB} = 10$ μm. This means that each 3 dB-coupler is $2L_{SB} + L_p$ long.

By observing Fig. 9(a) one can notice that for narrow silicon waveguides very small coupler lengths (L_p) are in general needed, especially for smaller gap values. This is because decreasing the waveguide width actually results in expanding the waveguide mode, thus favoring mode coupling and decreasing the coupling-length (L_c). Opposite to the narrow-ridge silicon waveguides, the wider-ridge ones exhibit very tight confinement, i.e., most of the power is residing inside the waveguide core. Consequently, very small gaps are required in order to effectively couple them with reasonable coupler lengths [Fig. 9(b)].

Commenting on the 3 dB-coupler design, several coupling-orders satisfying $L_p < 10$ μm are accessible for the

smaller gap values, and are marked on the respective curves of Fig. 9. The coupling-orders are identified by the number of times the input light is exchanged between the two arms before it is actually split. For a given gap value, the n'th coupling-order length is given by $L_{\mathrm{p}}^{(n)} \approx L_{\mathrm{p}}^{(0)} + nL_{\mathrm{c}}$, where $L_{\mathrm{c}} = 0.5\lambda/\Delta n_{\mathrm{eff}}^{\mathrm{S-A}}$ is the coupling length, extracted, e.g., from the effective-index difference of the symmetric and anti-symmetric TM supermodes of the coupler. $L_{\mathrm{p}}^{(0)}$ is the fundamental coupling-order length, for the specific gap value and S-bend parameters, which converges to $0.5L_{\mathrm{c}}$ for sufficiently large gaps. In this case, the BPM simulations are redundant, i.e., an eigenmode investigation of the coupler suffices. On the contrary, for very small gap values, the coupling at the S-bend sections is so strong that the fundamental coupling-order may not be accessible. From the technological viewpoint, it is generally safer to opt for relatively large gaps so that fabrication errors have a limited effect on the design performance. Finally, we note that the 3 dB-couplers feature a quite wideband performance. Specifically, the splitting-ratio (SR), that is ideally equal to 0 dB at the C-band central design wavelength of 1550 nm, did not exceed the value of 1 dB in a 100 nm window around 1550 nm. As intuitively expected, 3 dB-couplers based on the fundamental coupling-order yield the largest bandwidth.

5.2 Multi-Mode Interference Switch

We now focus on the hybrid SOI-DLSPP MMI switch [Fig. 8(b)]. As in the hybrid MZI case, the passive Y-splitters/combiners used to distribute/recombine the input/output power to/from the MMI section are implemented with SOI waveguides. Again, note that the MMI section is accommodated in a buried-oxide cavity providing the necessary vertical offset (250 nm) for efficient coupling between the two waveguides [Fig. 8(b)]. As described in Ref. 13, the wide DLSPP waveguide of the MMI section supports two modes, the fundamental symmetric TM_{00} mode and the anti-symmetric TE_{00} mode. When both modes are excited in the MMI input, the resulting mode-beating is characterized by a beating-length L_{B}. By heating the MMI waveguide we can change this beating length thus switching the output port. The length of the MMI section needed for the output-port switching, L_{MMI}, is inversely proportional to the thermally induced index-change in the polymer-loading, i.e. higher thermo-optic efficiency leads to smaller MMI lengths.

Apart from different phase-constants, the modes of the DLSPP MMI waveguide experience considerably different propagation losses as well. For the reference loading, the fundamental plasmonic mode (TM_{00}) is damped more than twice as fast as the higher-order, "photonic-like" mode (TE_{00}). This difference can limit the component's output-port ER: in order to completely eliminate the field in one of the output-ports, the beating modes must interfere at equal powers and at a phase-difference of π. Consequently, we need to properly design the input/output Y-junctions in order to excite the two modes in such a proportion that will eventually cancel out the aforementioned loss-difference along the MMI section. Assuming, for fabrication simplicity, that the input/output Y-junctions are identical, the optimized excitation ratio for both Y-junctions is given by the square-root of $R_{\mathrm{S/A}}$ in Ref. 13. An overall $R_{\mathrm{S/A}} > 1$ means that the combined effect of the input and output Y-junctions should favor the TM_{00} mode over the TE_{00}.

A simple and efficient Y-junction design is the one depicted in the bottom-right hand corner of Fig. 8, employing 170nm-wide silicon-wire feeds and a DLSPP taper section. The junction's parameters-to-optimize are three: the gap between the Si-arms at the wide interface of the DLSPP taper (d_{gap}), the taper length (L_{T}) and the taper width (W_{T}). Targeting the overall $R_{\mathrm{S/A}}$ of Ref. 13, a non-exhaustive optimization yielded the parameter-set $d_{\mathrm{gap}} = 1.2$ μm, $L_{\mathrm{T}} = 8$ μm and $W_{\mathrm{T}} = 1.5$ μm, for the particular Y-junction designs. Nevertheless, other Y-junction designs can be also identified, especially ones using different input/output configurations. In these approaches, the idea is to pursue a small $R_{\mathrm{S/A}}$ (< 1) at the input and a large one (> 1) at the output. Their product should be equal to the optimal value for the particular MMI waveguide, so that the beating-modes interfere at equal powers at the output, thus maximizing the ER. Additionally, the average propagation losses along the MMI section are reduced since the low-loss TE_{00} mode carries the majority of the signal power. However, our numerical investigations indicate that small value of excitation-ratio (< 1) always come at the cost of increased insertion losses at the Y-junction, thus negating the improvement in IL along the MMI section described above.

6. CONCLUSION

We have presented a comprehensive analysis of end-fire coupling between dielectric-loaded surface plasmon polariton (DLSPP) and compact rib/wire silicon-on-insulator (SOI) waveguides. The geometrical parameters leading to optimum performance, i.e., maximum coupling efficiency, have been identified. Coupling efficiencies as high as 85 % have been attained. In addition, we have assessed the effect of a metallic stripe gap and that of a horizontal offset between waveguides on insertion loss. Benefiting form the low-loss coupling between the two waveguides, we have demonstrated hybrid SOI-DLSPP 2×2 thermo-optic switching elements which outperform their all-DLSPP counterparts in terms of IL. In particular, the hybrid SOI-DLSPP MZI of Sec. 5.1 exhibits a 4.5-dB IL improvement with respect to the all-DLSPP component.

ACKNOWLEDGMENTS

This research has been co-financed by the European Union (European Social Fund – ESF) and Greek national funds through the Operational Program "Education and Lifelong Learning" of the National Strategic Reference Framework (NSRF) — Research Funding Program: Heracleitus II. Investing in knowledge society through the European Social Fund.

REFERENCES

[1] Bozhevolnyi, S. I., ed., [*Plasmonic Nanoguides and Circuits*], Pan Stanford Publishing, Singapore (2008).

[2] Oulton, R. F., Sorger, V. J., Genov, D. A., Pile, D. F. P., and Zhang, X., "A hybrid plasmonic waveguide for subwavelength confinement and long-range propagation," *Nat. Photon.* **2**(8), 496–500 (2008).

[3] Grandidier, J., Colas des Francs, G., Massenot, S., Bouhelier, A., Markey, L., Weeber, J.-C., Finot, C., and Dereux, A., "Gain-assisted propagation in a plasmonic waveguide at telecom wavelength," *Nano Lett.* **9**(8), 2935–2939 (2009).

[4] Gather, M. C., Meerholz, K., Danz, N., and Leosson, K., "Net optical gain in a plasmonic waveguide embedded in a fluorescent polymer," *Nat. Photon.* **4**(7), 457–461 (2010).

[5] Hochberg, M., Baehr-Jones, T., Walker, C., and Scherer, A., "Integrated plasmon and dielectric waveguides," *Opt. Express* **12**(22), 5481–5486 (2004).

[6] Berini, P., Charbonneau, R., Lahoud, N., and Mattiusi, G., "Characterization of long-range surface-plasmon-polariton waveguides," *J. Appl. Phys.* **98**, 043109 (2005).

[7] Degiron, A., Cho, S.-Y., Tyler, T., Jokerst, N. M., and Smith, D. R., "Directional coupling between dielectric and long-range plasmon waveguides," *New J. Phys.* **11**(1), 015002 (2009).

[8] Chen, X.-W., Sandoghdar, V., and Agio, M., "Highly efficient interfacing of guided plasmons and photons in nanowires," *Nano Lett.* **9**(11), 3756–3761 (2009).

[9] Delacour, C., Blaize, S., Grosse, P., Fedeli, J. M., Bruyant, A., Salas-Montiel, R., Lerondel, G., and Chelnokov, A., "Efficient directional coupling between silicon and copper plasmonic nanoslot waveguides: toward metal-oxide-silicon nanophotonics," *Nano Lett.* **10**(8), 2922–2926 (2010).

[10] Wu, M., Han, Z., and Van, V., "Conductor-gap-silicon plasmonic waveguides and passive components at subwavelength scale," *Opt. Express* **18**(11), 11728–11736 (2010).

[11] Briggs, R. M., Grandidier, J., Burgos, S. P., Feigenbaum, E., and Atwater, H. A., "Efficient coupling between dielectric-loaded plasmonic and silicon photonic waveguides," *Nano Lett.* **10**(12), 4851–4857 (2010).

[12] Tsilipakos, O., Kriezis, E. E., and Bozhevolnyi, S. I., "Thermo-optic microring resonator switching elements made of dielectric-loaded plasmonic waveguides," *J. Appl. Phys.* **109**(7), 073111 (2011).

[13] Pitilakis, A. and Kriezis, E. E., "Longitudinal 2×2 switching configurations based on thermo-optically addressed dielectric-loaded plasmonic waveguides," *J. Lightw. Technol.* **29**(17), 2636–2646 (2011).

[14] Hassan, K., Weeber, J.-C., Markey, L., Dereux, A., Pitilakis, A., Tsilipakos, O., and Kriezis, E. E., "Thermo-optic plasmo-photonic mode interference switches based on dielectric loaded waveguides," *Appl. Phys. Lett.* **99**(24), 241110 (2011).

[15] Gosciniak, J., Volkov, V. S., Bozhevolnyi, S. I., Markey, L., Massenot, S., and Dereux, A., "Fiber-coupled dielectric-loaded plasmonic waveguides," *Opt. Express* **18**(5), 5314–5319 (2010).

[16] Gosciniak, J., Bozhevolnyi, S. I., Andersen, T. B., Volkov, V. S., Kjelstrup-Hansen, J., Markey, L., and Dereux, A., "Thermo-optic control of dielectric-loaded plasmonic waveguide components," *Opt. Express* **18**(2), 1207–1216 (2010).

[17] Palik, E. D., ed., [*Handbook of Optical Constants of Solids*], Academic Press, New York, first ed. (1985).

[18] Kweon, G.-I. and Park, I.-S., "Splicing losses between dissimilar optical waveguides," *J. Lightw. Technol.* **17**(4), 690–703 (1999).

[19] Tsilipakos, O., Pitilakis, A., Tasolamprou, A., Yioultsis, T., and Kriezis, E., "Computational techniques for the analysis and design of dielectric-loaded plasmonic circuitry," *Opt. Quantum Electron.* **42**, 541–555 (2011).

[20] Tsilipakos, O., Kriezis, E. E., and Yioultsis, T. V., "Boundary condition for the efficient excitation and absorption of hybrid waveguide modes in finite element formulations," *Microwave Opt. Technol. Lett.* **53**(11), 2626–2631 (2011).